Performance Evaluation of Low-Thrust Rocket Nozzles of Various Geometries

Ahmad Hussein Abdul Hamid, Zuraidah Salleh*
High Energy Material Research Laboratory (HEMREL),
School of Mechanical Engineering, College of Engineering,
Universiti Teknologi MARA, Malaysia
**hussein@uitm.edu.my*

Ahmad Tamimi Ahmad Termizi, Mohamad Amirul Muhammad
MTC Defense, MTC Engineering Sdn Bhd

Mohd Azan Mohammed Sapardi
Department of Mechanical Engineering, Kulliyyah of Engineering,
International Islamic University Malaysia

ABSTRACT

Issues of viscous loss in rocket nozzle become increasingly more important as the thrust chamber is reduced in size. A properly designed nozzle is critical since small geometrical differences can result in dramatically modified performance. The present study analyzes the performance of conical converging-diverging nozzle for low-thrust rocket application. A total of five nozzles with different area ratio and divergence length were numerically tested; two optimum area ratio nozzles, one underexpanding nozzle and two overexpanding nozzles. The main aim is to analyze the flow phenomena of compressible gas flows within these nozzles and its relation to the rocket performance (i.e. thrust). The axisymmetric flow problems are numerically solved using a well-validated software with the Spalart-Allmaras turbulence model is employed to model the effect of turbulent on the flow. The results revealed technique of eliminating flow separation and obviously, knowledge of the point of separation is essential for performance enhancement. The elimination of flow separation inside the overexpanding nozzle by means of truncating it at a point of separation increases the thrust produced by 18% for a relatively low combustion pressure. It is anticipated that the thrust enhancement would be greater for a higher nozzle pressure ratio (NPR, i.e. the ratio of combustion chamber total pressure and atmospheric static

ISSN 1823-5514, eISSN 2550-164X
Received for review: 2021-02-17
Accepted for publication: 2021-11-15
Published: 2022-01-15

pressure). With the demonstrated performance enhancement, this work serves as a driver for further nozzle enhancement using this technique.

Keywords: *Converging-diverging Nozzle; Rocket; Supersonic; Shockwave; Thrust*

Introduction

Malaysia's interest in space missions was realized when the first national microsatellite, TiungSAT-1 was launched in 1998 into low Earth orbit on a Russian-Ukrainian Dnepr rocket. A major enabling technology for a space mission, i.e. satellite launching is aerospace propulsion, but unfortunately, Malaysia is left far behind in this field. Too dependent on other's technology to launch our own satellite means scheduling, priority, and the launcher cannot be available on short notice.

The aerospace propulsion system is a system in which the fundamental principle obeys the second and third Newton's law, namely that force is proportional to the rate of change of momentum, and that action and reaction are equal and opposite. One of the main components in the rocket propulsion engine is the rocket nozzle, which accelerates combustion gases as they leave the rocket and thereby maximize the thrust. Since the velocity is greater as it leaves the nozzle, its temperature and pressure will be reduced [1]. The nozzle configuration is determined by the geometrical shapes of the nozzle's divergent portion. Of many nozzle configurations, conical and bell shapes are widely used in the thrust chamber.

Arrington *et al*. [2] investigated the performance of both conical nozzle and bell nozzle for small thrust chamber (throat Reynolds number range from 20,000 to 40,000). They found that bell nozzle outperformed conical nozzle, regardless of the chamber pressure and the mixture ratio. The numerical investigation also indicates that the bell nozzle shows better performance than the conical nozzle [3]. However, the bell nozzle has the disadvantage of being expansive to manufacture as the shape has to be exact. Furthermore, to produce the axial discharge, the bell nozzle length has to be considerably greater than that of the corresponding conical nozzle, and the frictional loss due to this extra length may nullify the gain due to parallel flow.

A conical nozzle is the simplest to construct, and the divergence half-angle may be 12^{o} to 20^{o} [4,5]. Despite having low performance due to thrust loss by the non-parallel streamlines at discharge [6], several studies have shown that this nozzle outperformed the bell nozzle. A numerical and experimental investigation of low Reynolds number nozzle on different types of nozzle configurations and propellants showed that the conical nozzle outperform the bell nozzle experimentally and numerically regardless of the

types of propellant used [7]. Similar results were reported where the bell nozzles tested had efficiencies generally lower than the conical nozzles, irrespective of the area ratio [8]. The author also reported that the nozzles with higher area ratio have better efficiency compared to nozzles with smaller area ratio. In a more recent report, a weak oblique shock has been observed in the plume of an optimized conical nozzle [9]. More recent research by Jankovsky *et al*. [10] also revealed that a nozzle with a higher area ratio produces higher trust than a nozzle with a smaller area ratio. Yet, there are tradeoffs for high area ratio nozzle. Teasdale *et al*. [11] reported that the underexpanding nozzle is generally preferable than the overexpanding nozzle since the drag and non-axial component of the gas velocity are smaller. In addition, the weight of the nozzle with a high area ratio makes its application impractical [12].

The reasons for these observations are still lacking, particularly related to the flow phenomena inside a compressible conical converging-diverging nozzle for small thrust application. A recently developed code [13], for example, could not reproduce detailed shockwaves phenomena inside the nozzle. The present investigation seeks to numerically solve such flows and gain a better understanding of the important flow features in order to optimize the overall propulsion system. Furthermore, of all the cited references above, most of them dealt with the investigation of medium and high area ratio nozzle [5, 11-12], except for [10]. Reference [10] conducted an experimental investigation of a high area ratio (Ae/At = 1025) rocket nozzle due to the intended operation of orbital transfer vehicle (i.e. operating in a vacuum condition). Other examples of investigation on low area ratio nozzle are the ones done by Sun *et al*. [16] (nozzle area ratio of 6.6), Bayt *et al*. [17] (nozzle area ratio of 4.2), Wu *et al*. [18] (nozzle area ratio of 3.2), Xiao *et al*. [19] (nozzle area ratio of 1.5) and Khalid *et al*. [20] (nozzle area ratio of 0.5625). There have been relatively few investigations on low area ratio nozzle, and the present research is intentionally carried out to further study the performance of low area ratio nozzle (nozzle area ratio between 1.2 and 4). The nozzles are of conical contour since it offers significant advantages over the bell nozzle, both in ease in fabrication and performance.

Methodology

Computational work was carried out on four different nozzles to analyze the performance of the thrust chamber nozzles for a given nozzle pressure ratio (NPR). CFD analysis is more preferable at the development stage as it able to provide relatively accurate performance estimation with much lower cost compared to experimental analysis [21]. The four nozzles were designed with different area ratio (A_2/A_t) and divergence portion length. The first nozzle (nozzle 1) was designed to have an optimal expansion of combustion product

at the nozzle divergent part as it will produce theoretically maximum thrust. In this particular setup, the nozzle exit pressure is equal to the ambient pressure, i.e. $P_2 = P_3$. The performance of this nozzle was set as a benchmark for other nozzles. Second nozzle (nozzle T1) was a truncated nozzle 1, where the divergence part of the nozzle was 2 mm shortened from nozzle 1. The reason for truncating nozzle 1 is to analyze the effect of underexpanding nozzle on the flow performance. Third nozzle (nozzle 2) was designed to have the same area ratio as the first one but with greater divergence length. Fourth nozzle (nozzle 3) was designed to have a larger area ratio (overexpanding nozzle) with the same divergence length as the third one. All nozzles were investigated numerically under the assumption that the flow is compressible and axisymmetric. All nozzles had the same convergence angle of 40° since a study [22] showed that the upstream geometry of nozzle, which is the convergence portion has no impact on divergence loss.

A conical shaped nozzle, the most common contour for the thrust chamber nozzle [23] was chosen for all nozzles instead of an optimized bell nozzle contour to simplify the thrust chamber fabrication. Furthermore, the nozzle profile is not critical for good performance since the flow occurs in a region of favorable pressure gradient [24]. Several researches have shown that conical nozzle outperform bell nozzle regardless of nozzle area ratio and types of propellant used [2, 4-5]. Figure 1 shows the nozzle's geometrical shapes and the dimensions are tabulated in Table 1.

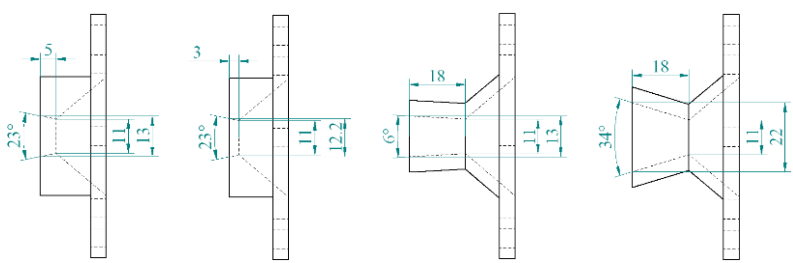

Figure 1: Nozzles with different geometry (all length dimensions are in mm).

Table 1: Nozzles dimensions

Parameter	Nozzle 1	Nozzle T1	Nozzle 2	Nozzle 3
Divergence angle, (°)	23	23	6	34
Divergence length	5	3	18	18
Area ratio (A_2/A_t)	1.4	1.2	1.4	4

The flow inside these nozzles was numerically simulated using FLUENT software that has been well validated against experimental data [25]. Since the nozzles have a circular cross-section, it is reasonable to assume that the flow is axisymmetric. Hence all nozzles geometry was created in two-dimensions to optimize computing time. Figure 2 shows the geometry and grid distribution inside nozzle 1. The grid density was higher in the divergent part of the nozzle and clustered at the nozzle exit to improve the resolution for capturing possible shocks.

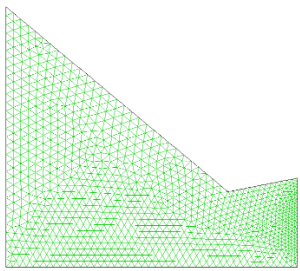

Figure 2: Grid distribution inside nozzle 1.

The density of grid cells is designed in such a way that the results are insensitive to it. This is crucial to eliminate the influence of grid size on the computational results. Table 2 summarizes the number of nodes and triangular cells for all nozzles.

Table 2: Number of nodes and cells for all nozzles

Nozzle	Number of nodes	Number of triangular cells
Nozzle 1	1422	2682
Nozzle T1	1542	2922
Nozzle 2	1536	2870
Nozzle 3	1579	2956

A grid independent study was conducted to ensure the solutions are insensitive to the mesh density. Nozzle 2 was chosen for this particular study since this nozzle has the largest wetted surface and poses the most demanding mesh refinement. Four different mesh densities were studied to allow testing for convergence. The results are summarized in Table 3 and revealed an error of less than 0.6% between meshes M4 (the finest mesh) and M3. Hence mesh density M3 is chosen for the present investigation.

Table 3: Average exit Mach number for nozzle 2

Nozzle	Number of nodes	Ma
M1	921	1.53
M2	1229	1.66
M3	1536	1.70
M4	1689	1.71

The problem is numerically solved using two-dimensional, axisymmetric, coupled solver (whereby the governing equations of continuity, momentum, and energy are solved simultaneously) and linearized using an implicit scheme. The coupled solver was recommended when dealing with applications involving compressible flows, and the governing equations were linearized using an implicit scheme for faster convergence than the explicit counterparts [26]. The working fluid is assumed to obey the ideal gas equation of state. Spalart-Allmaras turbulence model was employed given the fact that it has been shown to give good results for boundary layers subjected to adverse pressure gradients [27]. Furthermore, Charmeau et al. [28] cited that this one-equation model has shown relatively good accuracy in analyses of converging-diverging nozzles.

The inlet boundary conditions were imposed as follows: pressure and temperature at the nozzle inlet were set to be P_1 = 500 kPa and T_1 = 3400 K, respectively to represent the combustion pressure and temperature. The nozzle outlet pressure and temperature were set at 100 kPa and 2490 K, respectively. It should be noted that the initial outlet temperature is estimated assuming the flow is expanded isentropically inside the nozzle.

Results and Discussion

Computed Mach number and static pressure contours for nozzle 1, nozzle T1, nozzle 2 and nozzle 3 are shown in Figure 3, 4, 5 and 7, respectively. Note that the nozzle's throat is located at 0.016 m downstream of the nozzle inlet.

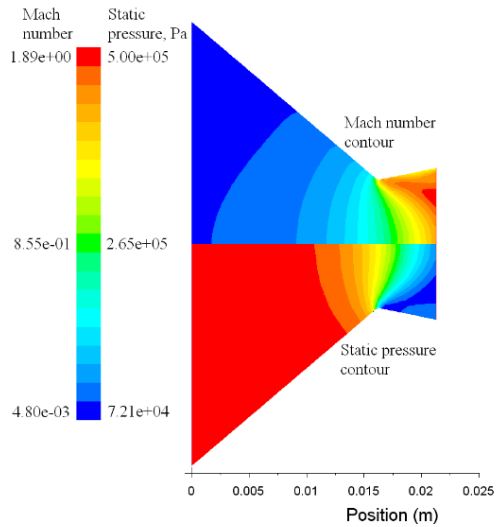

Figure 3: Mach number and static pressure contour of nozzle 1.

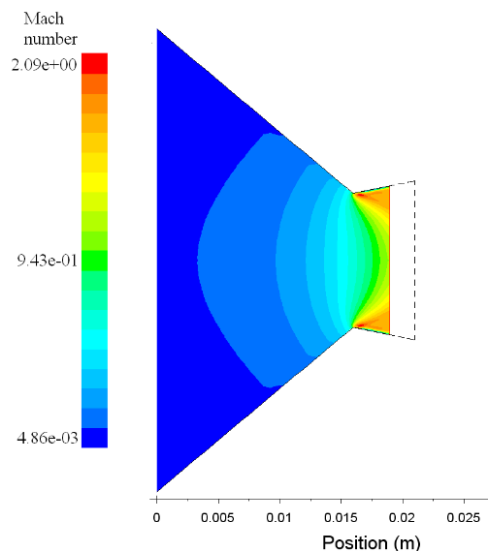

Figure 4: Mach number contour of nozzle T1.

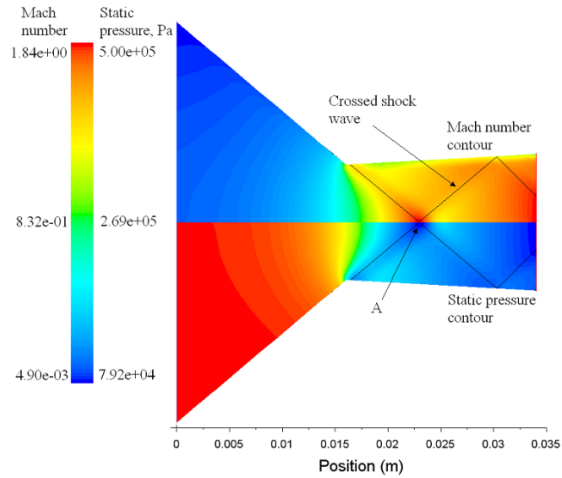

Figure 5: Mach number and static pressure contour of nozzle 2.

It was observed that the throat became sonic (Ma = 1) for all nozzles, shown by the supersonic condition at the divergence part of all nozzles. This condition is also known as a chocked condition, where the throat can carry no additional mass flow unless the throat is widened and it is a must for thrust chamber's nozzle to achieve this condition in order to gain thrust. Table 4 summarizes the Mach number and static pressure at nozzle exit for all nozzles.

Table 4: Exit Mach number and static pressure for all nozzles

Nozzle exit condition	Nozzle 1	Nozzle T1	Nozzle 2	Nozzle 3
Minimum Mach number	0.99	1.16	0.99	0.05
Maximum Mach number	1.89	1.77	1.84	3.45
Average Mach number	1.71	1.53	1.70	1.74
Minimum static pressure (kPa)	72.10	77.35	79.38	6.86
Maximum static pressure (kPa)	121.58	214.13	96.57	100
Average static pressure (kPa)	91.50	126.97	90.02	73.35

It can be seen from Figure 3 that there was no shock occurring inside nozzle 1. This observation can be explained by the fact that the flow exit pressure was less than the ambient pressure, and hence the shock may form at the outside of the nozzle. The flow expands to a pressure of 91.50 kPa, the closest to atmospheric pressure compared to the other nozzles (126.97 kPa, 90.02 kPa and 73.35 kPa for nozzle T1, nozzle 2 and nozzle 3 respectively).

This result was expected since nozzle 1 was designed to have an optimum area ratio. This expansion causes the flow to accelerate out of the nozzle at an average Mach number of 1.71. The expected thrust can be calculated by knowing the expected Mach number and design mass flow rate of propellant using the equation below:

$$F_e = \dot{m} V_e \tag{1}$$

where F_e and V_e are the expected thrust and velocity of flow at nozzle exit respectively, whereas $\dot{m}$ is the design propellant mass flow rate. For the sake of performance comparison, the propellant mass flow rate is approximated to be 0.029 kg/s based on the expected thrust of 50 N. Flow velocity and Mach number are related by the equation:

$$V_e = Ma \times a \tag{2}$$

where a is local sound speed, which is defined by the equation:

$$a = \sqrt{kRT} \tag{3}$$

where T is the average temperature of flow at the nozzle exit. The values of specific heat ratio, k and gas constant, R were taken from [12], which were 1.24 and 356.84 J/kg-K respectively. Table 5 summarizes the average flow temperature at the nozzle exit and the expected thrust for each nozzle.

Table 5: Flow temperature at nozzle exit and expected thrust for all nozzles

Nozzle	Average flow temperature at nozzle exit (K)	Expected thrust (N)
1	2157.94	48.46
T1	2327.83	45.03
2	2167.18	48.28
3	2134.20	49.04

From the equations above, the expected thrust for nozzle 1 is calculated to be 48.46 N, which is 3.1% less than the design thrust value of 50 N. It is anticipated that the expected thrust was very close to the designed thrust due to the fact that several correction factors have been considered in the calculation procedure for the propellant mass flow rate. The factors are velocity correction factor and thrust correction factor, which are 0.989 and 0.96, respectively. The velocity correction factor was considered to compensate the non-axial component of flow at nozzle exit, and the thrust

correction factor was considered to compensate other losses such as viscous loss, chemical kinetic loss and two-dimensional axisymmetric divergence loss.

Figure 4 shows the Mach number contour for nozzle T1. The dashed lines indicate its derivative geometry. It was observed that there is no shock occurred inside this nozzle too. The average static pressure at the nozzle exit was 126.97 kPa; slightly higher than the ambient pressure, which was expected since the length of the nozzle's divergence part is insufficient to allow the flow to completely expand to the ambient pressure. The average Mach number and the average temperature at the nozzle exit were 1.53 and 2327.83 K respectively, which results in the expected trust of 45.03 N. The expected thrust was 7.1% lower than for nozzle 1. However, the overall weight of the nozzle was reduced, which in turn increases the net thrust produced.

As for nozzle 2 (refer Figure 5), the lines inside the nozzle indicate the approximate position of oblique shock or crossed shock wave. These shocks were generated by the nozzle wall and intersected at point A in the flow. The shocks passed through each other and formed two additional shocks which then intersected and reflected from the nozzle wall. These intersections and reflection of shock waves from the nozzle wall produce a series of shocks known as crossed shock waves. Formation of shocks indicates that the downstream flow is supersonic. These shocks had caused the flow Mach number to increase along the centerline till the point of intersection at approximately Mach 1.88, and then it suddenly dropped abruptly to about Mach 1.3 before starting to increase until nozzle exit as shown in Figure 6. Wall 1 and wall 2 refers to nozzle divergence and convergence wall, respectively.

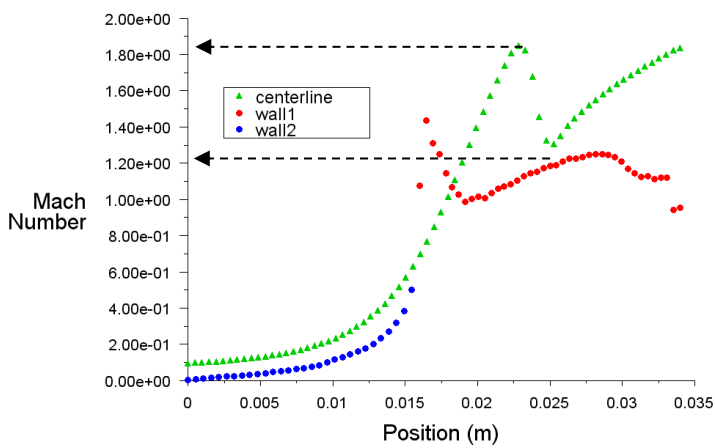

Figure 6: Mach number distribution along nozzle 2 centerline and walls.

In terms of performance, having same area ratio with nozzle 1, flow inside nozzle 2 expanded to an average pressure of 90.02 kPa, 1.62% less than nozzle 1 exit pressure. The average Mach number at the nozzle exit was 1.70, which in turn produced an expected thrust of 48.28 N; 0.4% less than for nozzle 1. One possible explanation is that the viscous drag on the nozzle walls increases as the nozzle's wetted surface is larger for a longer nozzle. It was reported that the lowest value of the divergence angle would result in lower total thrust [29] and a flow which is dominated by divergence loss [22]. However, in the present investigation, no significant thrust loss was observed by lengthening the nozzle while maintaining the area ratio.

In Figure 7, the separation of flow inside nozzle 3 due to the high area ratio was observed. The flow starts to separate from the nozzle wall at a distance of 28.2 mm from the nozzle inlet. Oblique shocks, which are formed from the nozzle wall due to the induced adverse pressure gradient, were observed inside the diverging section of the nozzle, which originated from the nozzle wall and is directed towards the nozzle centerline. The separation results in a free jet flow known as free shock separation (FSS) since no reattachment occurs downstream of separation location [30]. Consequently, a reversed flow region formed the downstream of the separation location, in which the ambient air is being sucked into the nozzle due to the low local pressure within the region. Figure 8 shows the velocity vector of the reversed flow region. Note that the length of the arrows represents the velocity magnitude, i.e. short arrows indicate a relatively low velocity.

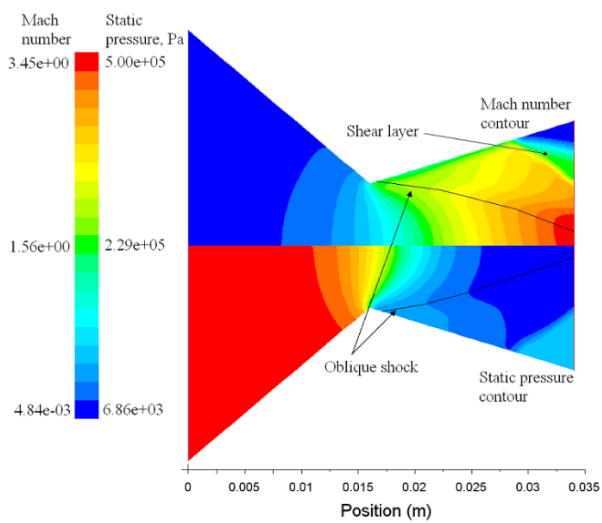

Figure 7: Mach number and static pressure contour of nozzle 3.

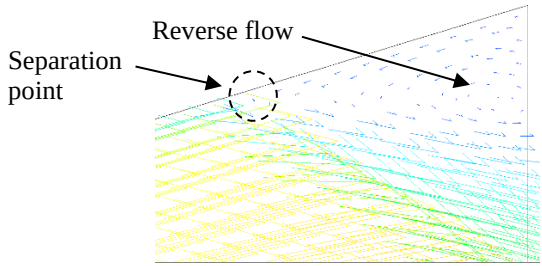

Figure 8: Velocity vector at the separated flow region.

By studying the pressure pattern in Figure 9, the flow can be divided into three regions. First; the upstream of incipient point, I, where the flow is attached to the nozzle wall. Second, where the pressure rises from incipient pressure (P_I) of about 30 kPa to the plateau with almost constant pressure (P_P). This region is referred to as a separation or interaction region. The flow separates from the wall at point S (separation point). The incipient pressure is the minimum wall static pressure, usually designated as the separation pressure, P_{sep} whereas plateau pressure corresponds to the wall pressure in the reverse flow region, which is the third region. The boundary layer starts to deflect at the incipient point, but it does not separate from the wall until point S, the separation point.

Expected thrust for nozzle 3 was 49.04, 1.2% higher than the one produced by nozzle 1. Ketsdever *et al*. [31] discussed that viscous effect was minimum at the largest divergence angle. This explains why nozzle 3 produces the highest thrust as compared to other nozzles. Previous researches are done by Whalen [8] and Jankovsky *et al*. [10] also revealed that nozzles with higher area ratio had better efficiency and produced higher trust compared to nozzles with smaller area ratio. The flow minimum static pressure at the nozzle exit was 6.86 kPa, which was far below the ambient pressure. It was because the nozzle geometry allows the supersonic flow to expand further in the nozzle divergence part until it reaches the exit plane.

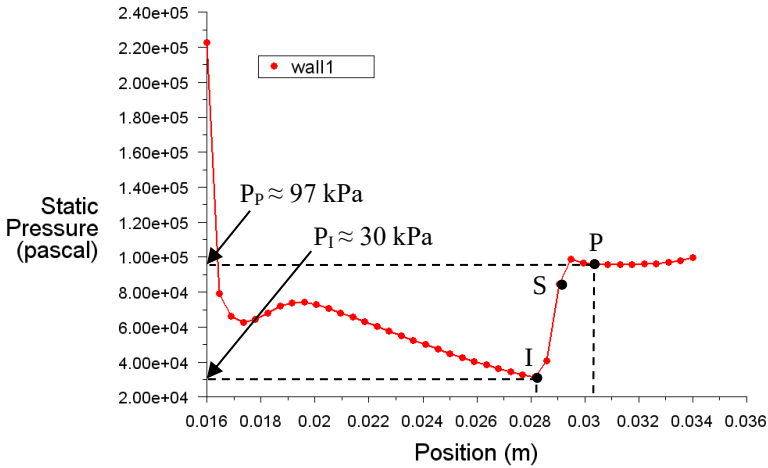

Figure 9: Static pressure distribution along nozzle 3 centerline and wall.

Referring to Figure 10, Mach number near the wall after the separation point was nearly zero as the flow was reversed at this region.

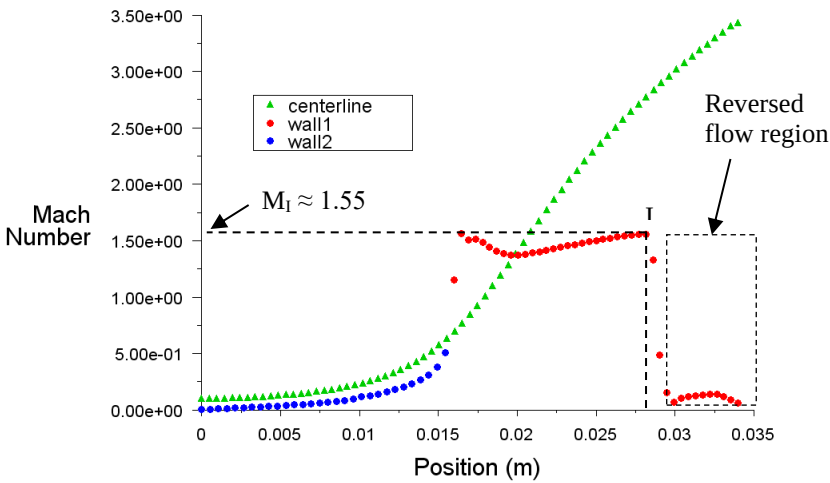

Figure 10: Mach number distribution along nozzle 3 centerline and wall.

It can be said that using the high area ratio nozzle does not give any significant increase in thrust (approximately 1% of increment). Furthermore, the extra thrust produced will be used to carry the additional weight of the high

area ratio nozzle. It has been reported that the nozzle performance can be further improved by shortening the diverging section length and that the effect is more prominence at a relatively lower Reynolds number [31]. In order to have benefited from the high area ratio nozzle and to eliminate the separation of flow, nozzle 3, which was truncated at the point of separation was analyzed. This truncated nozzle 3 (i.e. nozzle T3) has an area ratio of 3.3, 17.5% smaller than the original nozzle 3. Table 6 summarizes nozzle T3 dimensions. The flow condition at the nozzle exit, and the expected thrust is summarized in Table 7.

Table 6: Nozzle T3 dimensions

Parameter	Nozzle T3
Divergence angle (°)	34
Divergence length (mm)	12.2
Area ratio, A_2/A_t	3.3

Table 7: Nozzle T3 exit flow condition

Minimum Mach number	0.03
Maximum Mach number	2.85
Average Mach number	2.33
Minimum static pressure (kPa)	16.64
Maximum static pressure (kPa)	99.97
Average static pressure (kPa)	38.24
Average flow temperature (K)	1659.45
Expected thrust (N)	57.90

Simulation results revealed a minimum static pressure of nozzle T3 at nozzle exit of 16.64 kPa, which is 9.78 kPa higher compared to nozzle 3. This result was expected since the flow inside the truncated nozzle 3 was allowed to expand at a shorter distance compared to the flow inside nozzle 3. It was also observed that nozzle T3 produced the highest flow Mach number at the nozzle exit, which was 2.33. This, in turn, produced a thrust of 57.90 N, 18.07% higher than nozzle 3 and 19.48% higher than nozzle 1. This observation indicates that a nozzle with high area ratio and also one which allows the flow to expand more abruptly will produce high thrust provided that there is no flow separation occurring inside the nozzle (refer Figure 11). This observation also further strengthens the result found by Ketsdever *et al*. [31] that shortening the nozzle caused higher values of axial velocity at nozzle exit, which in turn results in higher thrust.

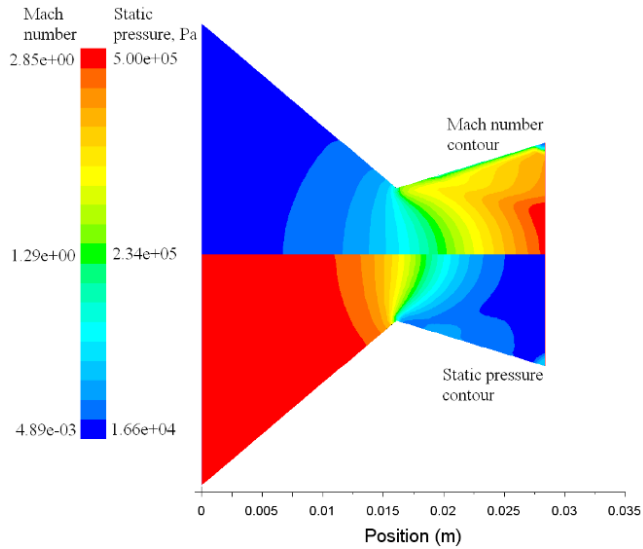

Figure 11: Mach number and static pressure contour of nozzle T3.

Conclusions

Fine nozzles with various area ratio and divergence length have been numerically investigated. One main conclusion is that elimination of flow separation inside the overexpanding nozzle by means of truncating it at a point of separation increases the thrust produced by as much as 18%. It is also important to mention that the truncated nozzles produce thrust higher than the theoretical value. Results also reveal that increasing the area ratio of the nozzle from 1.4 to 4 and that lengthening the nozzle while maintaining the area ratio does not give any significant changes in thrust produced, which is less than 2%. However, truncating the optimum area ratio nozzle causes noticeable loss in thrust, which is about 7%.

Acknowledgement

This publication was supported by the Micro-Industry Hub (MIH) Program (MIH-(005/2020)), a funded program under Universiti Teknologi MARA.

References

[1] E. K. S. Mohini, E. S. Mishra, and E. A. V. Yadav, "Performance Analysis of Converging Diverging Nozzle," *Int. Res. J. Eng. Technol.*, vol. 6, no. 9, pp. 24–29, 2019.

[2] L. Arrington, B. Reed, and J. Rivera Angel, "A performance comparison of two small rocket nozzles," in *32nd Joint Propulsion Conference and Exhibit*, 1996, pp. 2582.

[3] M. M. Hussaini and J. J. Korte, "Investigation of low-Reynolds-number rocket nozzle design using PNS-based optimization procedure," 1996.

[4] D. G. Shepherd, *Aerospace propulsion*. Elsevier Publishing Company, 1972.

[5] R. Ande and V. N. K. Yerraboina, "Numerical Investigation on Effect of Divergent Angle in Convergent-Divergent Rocket Engine Nozzle," *Chem. Eng. Trans.*, vol. 66, pp. 787–792, 2018.

[6] A. K. Mubarak and P. S. Tide, "Design of a double parabolic supersonic nozzle and performance evaluation by experimental and numerical methods," *Aircr. Eng. Aerosp. Technol.*, vol. 91, no. 1, pp. 145–156, 2018.

[7] S. Grisnik, T. Smith, and L. Saltz, "Experimental study of low Reynolds number nozzles," in *19th International Electric Propulsion Conference*, 1987, pp. 992, 1987.

[8] M. V Whalen, *Low Reynolds number nozzle flow study*. University of Toledo, 1987.

[9] C. Jéger and Á. Veress, "Novell Application of CFD for Rocket Engine Nozzle Optimization," *Period. Polytech. Transp. Eng.*, vol. 47, no. 2, pp. 131–135, 2019.

[10] R. S. Jankovsky, J. M. Kazaroff, and A. J. Pavli, "Experimental performance of a high-area-ratio rocket nozzle at high combustion chamber pressure," 1996.

[11] D. Teasdale, V. Milanovic, P. Chang, and K. S. J. Pister, "Microrockets for smart dust," *Smart Mater. Struct.*, vol. 10, no. 6, pp. 1145, 2001.

[12] G. P. Sutton and O. Biblarz, *Rocket propulsion elements*. John Wiley & Sons, 2016.

[13] A. J. Juhasz, "Converging-Diverging Nozzle Thruster Code for Nuclear or Chemical Rocket Performance Computations," *NASA/TM—2019-220164*, no. April, pp. 1–18, 2019.

[14] S. H. Morren, R. M. Myers, S. E. Benko, L. A. Arrington, and B. D. Reed, "A laboratory model of a hydrogen/oxygen engine for combustion and nozzle studies," *NASA Technical Memorandum 106281*,pp. 1-36 1993.

[15] A. Soi, "Dual Diverging Annular Rocket Nozzle (Focusing Flow Separation and Minimizing Overexpansion)," *Int. J. Sci. Res.*, vol. 6, no. 4, pp. 694–701, 2017.

[16] X. Sun and J. Wang, "Numerical Study of Supersonic Film Cooling in

Diverging Section of Nuclear Rocket Laval Nozzle," in *Proceedings of the 2018 26th International Conference on Nuclear Engineering ICONE26*, 2018, pp. 1–5.

[17] R. Bayt, A. Ayon, K. Breuer, R. Bayt, A. Ayon, and K. Breuer, "A performance evaluation of MEMS-based micronozzles," in *33rd Joint Propulsion Conference and Exhibit*, pp. 3169, 1997.

[18] K. Wu and H. Dong Kim, "Numerical study on the shock vector control in a rectangular supersonic nozzle," *Proc. Inst. Mech. Eng. Part G J. Aerosp. Eng.*, vol. 233, no. 13, pp. 4943–4965, 2019.

[19] Q. Xiao, H.-M. Tsai, and D. Papamoschou, "Numerical investigation of supersonic nozzle flow separation," *AIAA J.*, vol. 45, no. 3, pp. 532–541, 2007.

[20] M. W. Khalid and M. Ahsan, "Computational Fluid Dynamics Analysis of Compressible Flow Through a Converging-Diverging Nozzle using the k-ε Turbulence Model," *Eng. Technol. Appl. Sci. Res.*, vol. 10, no. 1, pp. 5180–5185, 2020.

[21] R. Ramesh Kumar and Y. Devarajan, "CFD simulation analysis of two-dimensional convergent-divergent nozzle," *Int. J. Ambient Energy*, vol. 41, no. 13, pp. 1505–1515, 2020.

[22] J. B. Pearson, D. B. Landrum, and C. W. Hawk, "Parametric study of solar thermal rocket nozzle performance," *J. Sol. energy Eng.*, vol. 118, no. 3, pp. 194-195, 1996.

[23] M. Almqvist, "Semi-empirical model for supersonic flow separation in rocket nozzles." 2005.

[24] R. A. Nakka, "Solid propellant rocket motor design and testing." University of Manitoba, 1984.

[25] A. K. Reji, G. Kumaresan, A. S. Menon, J. Parappadi, A. P. Harikrishna, and A. Mukundan, "Simulation and validation of supersonic flow through a convergent-divergent nozzle," *Int. J. Pure Appl. Math.*, vol. 119, no. 12, pp. 2135–2142, 2018.

[26] F. T. Guide, "Modeling External Compressible Flow," *Fluent Inc*, 2003.

[27] F. U. Guide, "Modelling Turbulence," *Fluent Inc*, 2003.

[28] A. Charmeau and S. Anghaie, "A Hybrid Fine-Coarse Computational Mesh Simulation Tool for Space Nuclear Systems," in *Proceedings of the Space Nuclear Conference*, 2005.

[29] T. I. M. S. B. Zaman, M. E. Hoque, and F. Rashid, "Investigating the Effect of Various Angles of Divergence of A Conical Rocket Nozzle During Boost Phase," in *International Conference on Mechanical Engineering and Renewable Energy 2019 (ICMERE2019)*, vol. 2019, pp. 1–4, 2019.

[30] S. B. Verma, R. Stark, and O. Haidn, "Relation between shock unsteadiness and the origin of side-loads inside a thrust optimized parabolic rocket nozzle," *Aerosp. Sci. Technol.*, vol. 10, no. 6, pp. 474–

483, 2006.
[31] A. D. Ketsdever, M. T. Clabough, S. F. Gimelshein, and A. Alexeenko, "Experimental and numerical determination of micropropulsion device efficiencies at low Reynolds numbers," *AIAA J.*, vol. 43, no. 3, pp. 633–641, 2005.